Multi-directional bubble generated streaming flows

Tamsin A Spelman, Olivier Stéphan, Philippe Marmottant

Multi-directional bubble generated streaming flows

Tamsin A. Spelman[a,b] [1], Olivier Stephan[c] and Philippe Marmottant[c]

[a] *School of Mathematics and Statistics, University of Glasgow, Glasgow, G12 8QQ, United Kingdom.*

[b] *DAMTP, University of Cambridge, Cambridge, CB3 0WA, United Kingdom.*

[c] *Univ. Grenoble Alpes and CNRS, UMR 5588 LIPhy, F-38402 Grenoble, France.*

Abstract

In previous work, we have demonstrated the use of single-holed Armoured Microbubbles (AMBs) for microfluidic mixing and self-propulsion. AMBs are hollow partial spheres, inside which we capture a bubble. Under ultrasound, the bubble oscillates, generating a streaming flow with velocities of $1 - 100$ mms^{-1} in water. In this paper, inspired by our successful fabrication of a C60 geometry (buckyball), we study AMBs with multiple surface holes. We show more holes generate additional pairs of fast circulations around the AMB. However, as the number of holes increases further, the circulations become small and the in-plane flow is dominated by a source or sink flow. For an AMB with two different sized holes, we demonstrate each hole can be independently activated, potentially useful for multi-directional swimming.

Keywords: microbubble, streaming, self-propulsion, mixing

1. Introduction

The powerful flows generated by ultrasound actuated microbubbles offer fantastic opportunities for microfluidic and biomedical applications, including targeted drug delivery [5] (since ultrasound is biologically safe at reasonable levels). These streaming flows have already been utilised for: microfluidic mixing [2, 21]; particle transportation - both directly by propelling the particle in microbubble generated streaming flows [14, 15] and indirectly by using the streaming flow to pull an object towards a microbubble so that

[1] Email: Tamsin.Spelman@slcu.cam.ac.uk. Current Address: Sainsbury Laboratory, University of Cambridge, CB2 1LR, United Kingdom

they become attached and the microbubble carrier, with its cargo, can then be propelled by alternative methods [6]; particle sorting [18, 22]; rupturing membranes [13] and self-propulsion [4]. Microbubbles focus ultrasound of wavelengths around 1 mm, down to the microscale [14], thus facilitating small scale manipulation, while still producing velocities on the order of millimetres per second. These microbubble streaming flows has also been extensively studied mathematically [8, 11, 12, 20, 17].

In recent work, we introduced armoured microbubbles (AMBs) [3, 4]. An AMB is a hollow partial sphere, which is built on a small tower attached to a coverslip using two-photon polymerisation (see Fig. 1a). A bubble is caught inside the open capsule when it is submerged in water, since capillary forces prevent water from entering the tiny hydrophobic capsule opening. When subjected to an ultrasound field, the bubble oscillates generating net motion in the fluid (a streaming flow), consisting of a strong jet, with velocities of $1-100$ mms^{-1} observed near the capsule opening. When the tower height, H, is short the coverslip influences the flow, and for $H = 10$ μm we observe a pair of fast circulations on either side of the strong jet near the capsule opening along with a weaker pair of circulations behind the AMB (see Fig. 1b). We showed the AMB can self-propel when broken off from its tower, using this strong jet it generates [4]. Self-propulsion by partially encased microbubbles has also been demonstrated by other authors, for larger bubbles [1] and larger cylindrical bubbles [9]. We extended this work to multi-propulsor compounds, including a triple-propulsor (see Fig. 1c), which generated three pairs of circulations around the AMB (see Fig. 1d). We also successfully used arrays of AMBs printed onto the base of a microfluidic channel for mixing two streams of fluid [3].

Over time, the fabrication technique has been honed, and thus we have recently been able to fabricate more complicated structures such as a C60 geometry, popularly known as a buckyball, (see Fig. 2a). In this paper, we use the refined setup to study AMBs with multiple holes. In §2, we outline our methodology. In §3, we analyse the streaming flow generated by an AMB with two equally sized holes before extending this to more holes arranged in regular 3D patterns on the capsule surface in §4. In §5, we analyse in detail, the effect of increasing the number of holes on the capsule surface by adding them to the central plane, where we focus the microscope. Finally, in §6, we consider an AMB with two different sized holes and determine whether they can be independently activated.

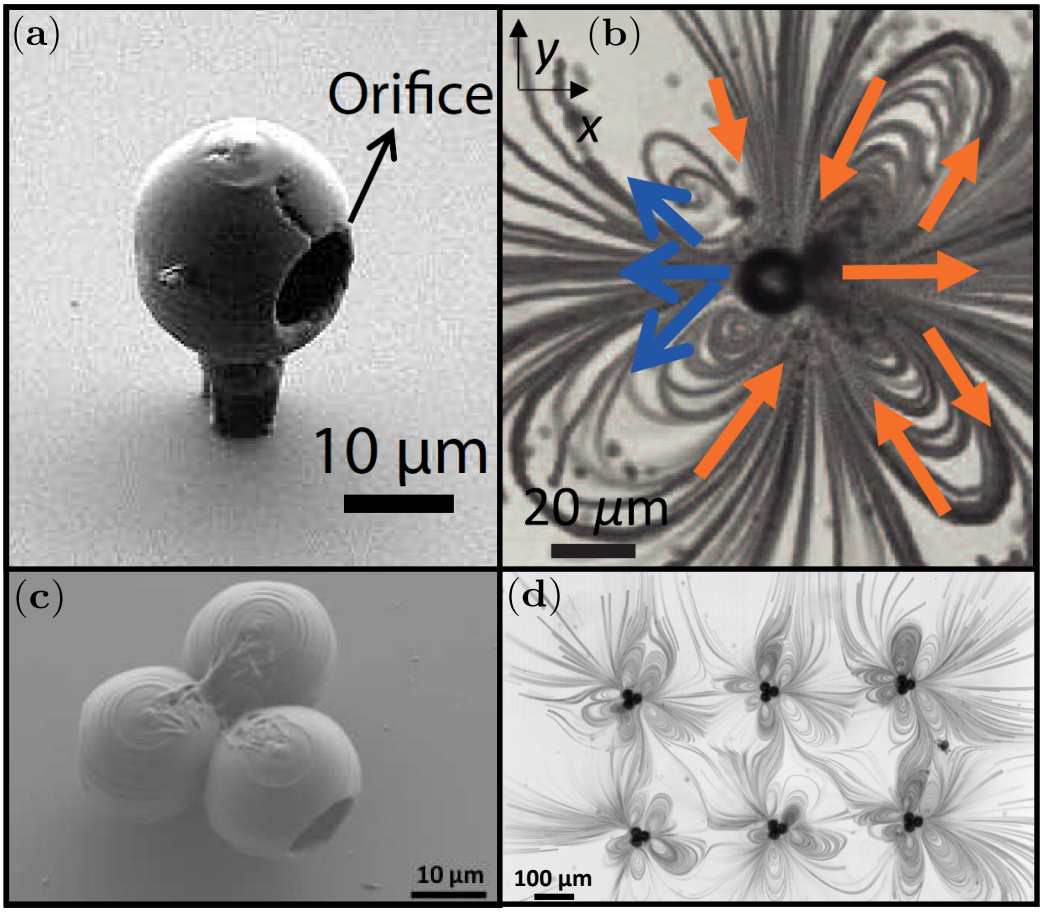

Figure 1: Illustration of the original single-hole AMB and the extension to multi-propulsor compounds. (a) SEM image of a single-hole AMB. (b) Streaming flow around a single-hole AMB. (c) Triple propulsor consisting of three attached single-hole AMBs on one tower. (d) Streaming flow around a triple propulsor. Fig. 1a and 1b are reproduced from N. Bertin et. al, Propulsion of bubble-based acoustic microswimmers, Phys. Rev. Applied, 4:064012, 2015 [4]. Fig. 1c and 1d reproduced from N. Bertin et. al, Bubble-based acoustic micropropulsors: active surfaces and mixers, Lab Chip, 17:15151528, 2017 [3].

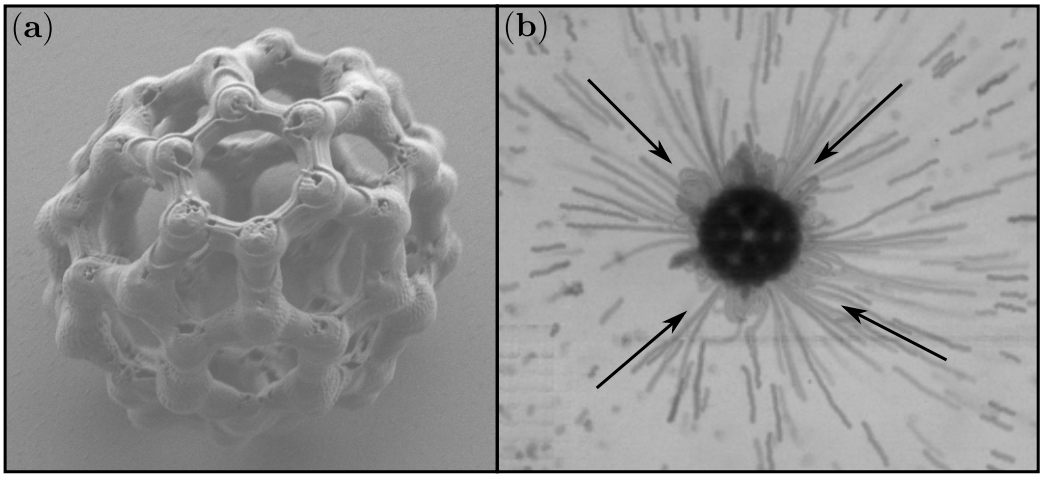

Figure 2: C60 geometry (buckyball) (a) SEM image of a fabricated C60 (b) Streaming flow generated by the C60 under ultrasound forcing.

2. Methodology

Our multi-hole AMBs are fabricated using a two-photon polymerisation setup, similar to that used for single-hole AMBs [4, 3]. We used Ormocomp resin [16], which polymerises under visible light at the 532 nm wavelength of a Nd:YAG microchip laser. The setup is based on an inverted microscope (100 X oil objective) and the two-photon absorption, which is localised in a small volume (around 1 μm^3) at the focal point. Three-dimensional (3D) patterning can be achieved by scanning the focal point in a drop of the photosensitive resin deposited on a microscope glass slide (25x25 mm^2). After microfabrication, the unreacted material is washed away using acetone leaving the 3D AMBs on top of the glass. The specific photosensitive resin is prepared with 6 mg 1,3,5-tris(2-(9-ethylcabazyl-3)ethylene)benzene, acting as a photoinitiator, dissolved in 1 mL dichloromethane and mixed with 1 g of Ormocomp. After stirring this mixture for one hour, the vial is opened for four additional hours (without stirring) in order to let the excess dichloromethane evaporate. The resin can then be stored for several weeks in the absence of light and moisture.

Our spherical multi-hole capsules were constructed on small towers of height 10 μm and radius 2 μm. In general, our capsules had a 10 μm outer radius and were 1 μm thick, with the holes having an aperture radius of 5 μm. We chose these relative sizes as previous work [3] reported that an aperture

radius to inner capsule radius ratio of approximately 0.5 is optimal for bubble lifespan on a single hole AMB. Where our capsule or aperture radius deviates from these dimensions, we will make specific reference. Capsules of this size took approximately $10 - 20$ min to fabricate, with more holes reducing the fabrication time.

To analyse the streaming flow, the capsules were contained in a small polydimethylsiloxane (PDMS) cell containing phosphate buffer solution (PBS) mixed with tracer particles of radius 1 μm , which was in turn contained within a larger tank of PBS. A transducer generated the ultrasound wave and a Phantom v2511 high-speed camera recorded the videos. This setup is similar to that used for single-hole AMBs [4]. For each velocity analysis, particle tracking was performed for each hole, on each AMB separately, using FAST software [7], in a rectangular analysis box of size $57\,\mu m \times 30\,\mu m$, with the long axis aligned with the direction the aperture hole points and one short side centred on the AMB centre (encompassing approximately $5\,\mu m$ to either side of the AMB at its widest point and $47\,\mu m$ in front of the AMB aperture).

To theoretically calculate the resonances of an AMB with two axisymmetric regions of bubble surface we used a potential model, following a similar method to that used to calculate the resonances of a single-hole AMB [19]. In brief, we assume an axisymmetric spherical body with mixed boundaries and negligible internal density, undergoing small amplitude oscillations where the radial position of the surface R, at azimuthal angle θ, is given by

$$R(\theta) = a\left(1 - \epsilon i \sum_{n=0}^{\infty} V_n P_n(\mu) e^{i\omega t}\right), \tag{1}$$

at time t, for angular frequency ω and spherical body radius a, where $\mu = \cos(\theta)$ and P_n are Legendre polynomials. The oscillations are assumed of small amplitude ϵa, and V_n are unknown constants which define the mode shape. On bubble surface the surface stress is balanced by surface tension and on solid surface there is no radial motion giving simplified eigenvalue equations of

$$\begin{cases} \sum_{n=0}^{\infty} V_n P_n(\mu)\left[\frac{\Omega}{n+1} - (n-1)(n+2)\right] = 0 & \theta \in \Theta_0 \\ \sum_{n=0}^{\infty} V_n P_n(\mu) = 0 & \theta \in \Theta_1 \end{cases}, \tag{2}$$

where the eigenvalue $\Omega = \rho a^3 \omega^2/\gamma$ for external fluid density ρ and surface tension γ, and where Θ_0 is the angles of bubble surface and Θ_1 solid surface.

To solve numerically we take the inner product, integrate over θ, truncate at $n = 1000$ and solve the linear generalised eigenvalue problem. For our two-hole AMB the aperture openings are of angle θ_0 and θ_1 (where $\theta_0 = \theta_1 = 0.52$) then $\Theta_0 = [0, \theta_0] \cup [\pi - \theta_1, \pi]$ and $\Theta_1 = [\theta_0, \pi - \theta_1]$. We assume dimensional values of $\rho = 10^3$ kgm^{-3}, $\gamma = 69.7 \times 10^{-3}$ Nm^{-1} and $a = 10^{-5}$ m. (Dimensional resonant frequency f is calculated as $f = \sqrt{\Omega\gamma/\rho a^3}/2\pi$).

To theoretically determine the streaming flow around a two-hole AMB we use the model we have previously derived for the streaming flow around an oscillating spherical body [20]. We have previously applied this to a AMB with a single hole [4, 19]. We can now apply this model to our two-hole AMB by imposing appropriate boundary conditions. On both bubbles caps $0 \leq \theta \leq \theta_0$ and $(\pi - \theta_1) \leq \theta \leq \pi$ we impose normal stress balanced by surface tension and no tangential stress. Between the caps ($\theta_0 < \theta < \pi - \theta_1$) we impose no radial or tangential velocity. Our model calculates the streaming flow around the AMB in free-space and then incorporates the wall by adding the images of the leading order Stokeslet and next order Stresslet.

The analytic model [20] for the streaming flow is axisymmetric so cannot be used directly to calculate the streaming flow around AMBs with more than two holes (and only if both holes are at the poles). To theoretically determine the streaming flow around an AMB with more than two holes, we assume each hole is independent and neglect all interactions between holes. Previously, we have successfully extended our model for the streaming flow around an AMB with a single-hole [4, 20] to study triple propulsors (Fig. 1c), by linearly superposing the streaming flow of each of the three individual AMBs [3], and we use a similar method here. For $\underline{u_i}(\underline{x}, t)$ the streaming flow generated by a single hole AMB, centred at the origin, with a hole in direction i, we use linear superposition to calculate the total streaming flow generated by the multi-hole AMB, centred at the origin, with n holes pointing in directions $i_1 ... i_n$ as $\sum_{k=1}^{n} \underline{u_{i_k}}(\underline{x}, t)$.

3. AMBs with two equally sized holes

Our first multi-hole capsule has two holes, placed on opposite sides of the AMB (see Fig. 3). Its streaming flow contains two strong jets, one at each aperture opening with each flanked by a pair of circulations (Fig. 3c), in agreement with our theoretical prediction (Fig. 3d). While the streaming is very similar in shape to the streaming around a single-hole AMB, the major difference is that the the jet at the front and back of the AMB are both

strong and have comparable strength. (Note, we obtain the same major flow features of Fig. 3d if we alternatively use our linear superposition analytic method.)

The largest velocities in the jets were observed at 290 kHz, with the best fit bell curve maximal at 315 kHz (see Fig. 3e), showing only a slight decrease in resonance frequency from a single hole. Previously, the resonance of a single hole AMB was experimentally calculated as 320 kHz [4], and an axisysmmetric analytic study, which predicted the resonance at 334 kHz, suggested this corresponded to a mode one vibration pattern [19]. Our two-hole potential model predicts a resonance at 324 kHz and 341 kHz corresponding to in-phase and out-of-phase mode one oscillations of both holes. Only one resonant mode is visible experimentally rather than two but experimental noise and band width could overlap these two very close modes, so they are not individually distinguishable experimentally. (Further, in Appendix A, we theoretically consider how the two resonances are effected as the angle between two bands on a spherical surface is changed, but such a case is not possible experimentally.) This suggests that the holes are influencing each other but not significantly enough to be impacting their streaming flow.

Thus, this two-hole AMB provides a method of producing two powerful jets and four circulations in the fluid. An alternative way to produce the same flow would be with a multi-propulsor compound, but the two-hole AMB has the advantage in being much smaller as all the holes are contained on one 10 μm capsule and having a faster fabrication time.

4. 3D Multi-hole armoured microbubbles

Having now understood two-hole streaming, we will increase the number of holes on our capsule surface. To maintain a regular array of holes, we considered holes placed at the vertices of each of the five regular polyhedra, giving AMBs with 4-holes, 6-holes, 8-holes 12-holes and 20-holes. We chose regular positioning for the holes as we hypothesised that the large number of symmetries would give similar flows in multiple directions.

The streaming behaviour observed for the four, six and eight hole AMBs have many similarities as seen in Fig. 4. Circulations are visible close to the AMB, and further away there is a dominance in flow being pulled towards the AMB, thus making the AMB act like a sink (in the focus plane of the microscope). This suggests significant out-of-plane motion to conserve mass,

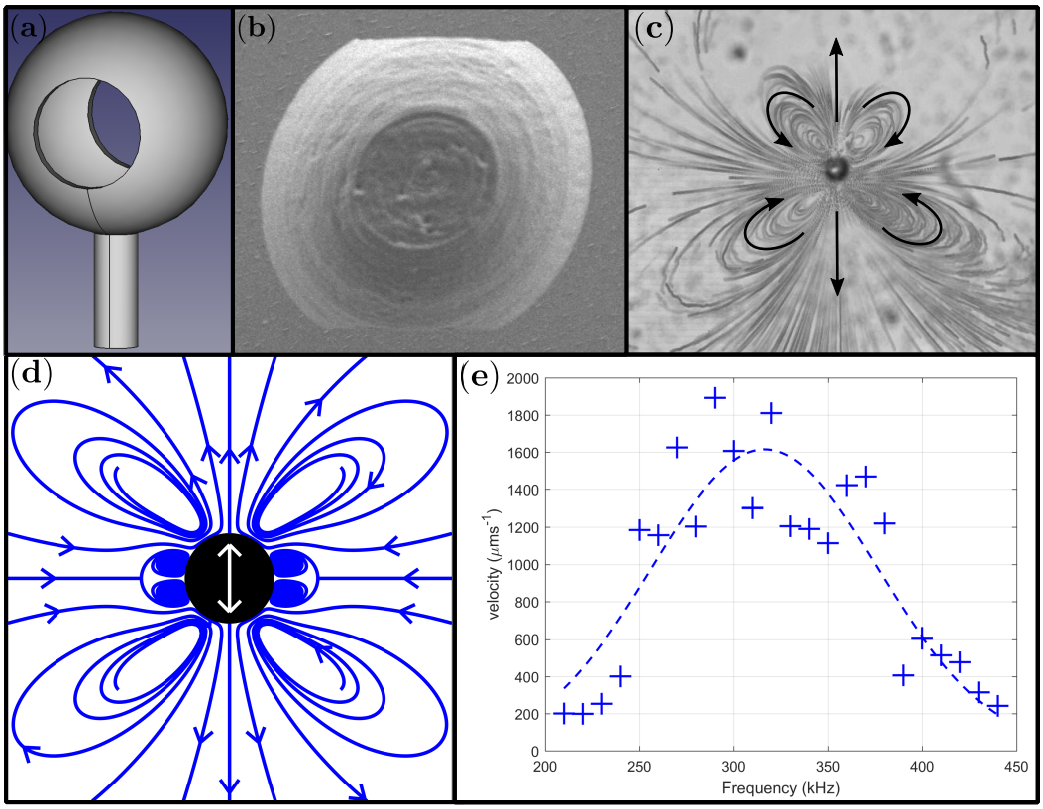

Figure 3: AMB with two equally sized holes. (a) FreeCAD design of the AMB. (b) SEM top down image of a two-hole AMB. The holes are positioned at the top and bottom of the image. (c) Experimental streaming flow around the two-hole AMB at ultrasound driving frequency of 330 kHz. (d) Theoretical streaming flow measured in a plane parallel to the wall through the centre of the AMB. (e) Velocity variation with increasing driving frequency, averaged over three AMBs and six holes, with velocity measured in a rectangular analysis box in front of each hole . Crosses indicate experimental data and a bell curve of best fit is plotted through this data.

which is unsurprising as the holes and their anticipated outward jets are out-of-plane. Looking specifically at the four-hole AMB, we can see the sink flow focussing in at three equally spaced locations, echoing the three holes angled towards the wall and the three-fold symmetry of the design. Between each jet are two circulations (although the circulations at the bottom of Fig. 4a are less well defined), which correlates with two circulations for each of the three holes angled towards the wall (which is the number and position of circulations we normally observe in front of a single hole).

The streaming flows also reflect the capsule symmetries, with the four-hole and six-hole AMBs having their three-fold rotational symmetry reflected in the streaming flow. The eight-hole AMB streaming flow should theoretically have four-fold rotational symmetry. This is partially represented with flow being pulled in from all sides and circulations all around the AMB, but there is a preferential direction for one axis. This lack of symmetry can be attributed to either tracer particles blocking holes or imperfections in the fabrication as the greater number of holes weaken the structure, both of which also support the observation that with more holes a higher proportion of capsules do not display the expected symmetries in their streaming flow.

The issue of tracers becoming trapped at the aperture openings of the AMB becomes more problematic with more holes, as a greater proportion of the surface is bubble rather than solid, so there is greater bubble surface area for the tracers to effect and less solid surface to protect the openings. Particular problems arose with AMBs containing six holes or more, which was reflected in the system losing symmetry after a short period of time, with the flow developing into a jet.

On the eight-hole capsule, the holes are tightly packed, and for our twelve and twenty hole designs we cannot fit sufficient holes of radius 5 μm on an AMB of 10 μm radius. For twelve holes, we increased the AMB radius to 12 μm. For twenty holes, we increased the radius to 17 μm and, to add more support, changed the dimensions of the associated tower to 3 μm in radius and 9 μm in height. However, these designs were structurally weak and the SEM images showed the washing process disfigured or crushed them, which was reflected in ultrasound experiments where streaming was visible but strongly favoured certain directions and sides of the capsule.

We next tested under ultrasound our C60 geometry (see Fig. 2a), which motivated this study. The geometrical shape consists of twelve pentagons and twenty hexagons, with each pentagon surrounded by five hexagons and each hexagon bordered by three pentagons and three hexagons. Our C60 has

hexagons with a radius of approximately 4.3 μm and pentagons with a radius of approximately 3.5 μm. These sizes was chosen to be close to the radius of our standard AMB holes while maintaining structural stability. We printed our C60 directly onto the coverslip so it sits on one of its faces, without a tower. Due to the smaller hole size, we used smaller tracer particles of radius 0.5 μm. Under ultrasound, the experimental flow field showed flow being pulled in slowly from all sides (see Fig. 2b) with small circulations close to the structure, similar to our spherical multi-hole AMBs. The streaming flow changes over time, suggesting the same problem with tracer particles as we observed with the multi-hole AMBs.

The frequencies at which the strongest velocities were observed near the AMB varied with the number of holes on the AMB, but the value oscillated around the 320 kHz resonance of the single hole AMB with the same size of aperture opening. For AMBs with a higher number of holes, the frequency producing the strongest velocities varied more widely between each specific capsule, suggesting interference from tracer particles or structural imperfections. However, the resonance for the four-hole AMB was observed at around 310 kHz and within the range $310 - 340$ kHz. For six-holes it was observed at around 320 kHz, and with eight-holes between 300 kHz and 360 kHz.

5. Planer armoured microbubbles

To better understand how the streaming flow changes as the density of holes on the AMB surface increases, we now study how the flow varies as the number of equally spaced holes centred on the central plane is increased, thus focusing the impact of the holes on the focus plane of the microscope.

From §3, we know that with two in plane holes we see the expected two pairs of circulations. As we increase this to three holes, we see the number of pairs of long and thin circulations increase to three in agreement with our theoretical prediction (see Fig. 5a). Experimentally two of the three pairs of circulations show saddles behind them (to the left and bottom right of the streaming flow in Fig. 5a), with source flow beyond (which is not predicted theoretically). This indicates the circulations having less influence further from the AMB. Also, since the presence and distance of these saddles from the AMB differs for each hole, this indicates a slightly more unstable flow field, with this feature likely dependent on previously less influential characteristics such as tracer particles or structural imperfections (since theoretically we expect a three-fold rotationally symmetric flow field).

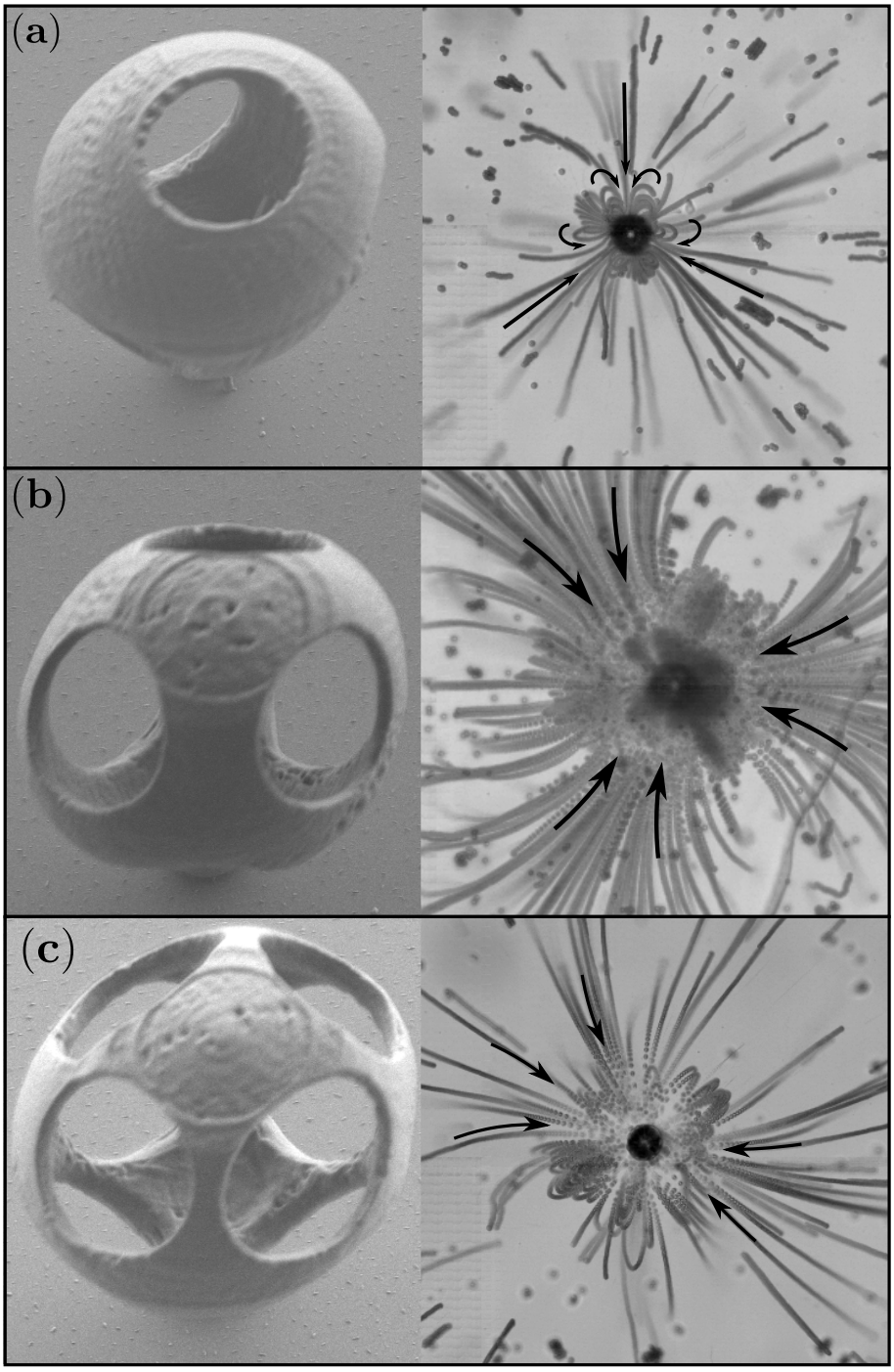

Figure 4: 3D multi-hole AMBs. (a) SEM image of a four-hole AMB and its streaming flow at 330 kHz. (b) SEM image of a six-hole AMB and its streaming flow at 290 kHz. (c) SEM image of an eight-hole AMB and its streaming flow at 330 kHz.

This flow structure is very similar to the triple propulsor (see Fig. 1d) and thus offers an alternative, smaller design to generate such a flow field.

As the number of holes is increased to four, the dominance of the circulations decreases further so they are now very small, with the source flow dominating (see Fig. 5b). This agrees with the theoretically predicted flow field, although theoretically four pairs of circulations are predicted, yet experimentally the number is unclear, likely due to their small size. Similar to three-hole AMBs, we also see some differences between the holes, where here we see one hole (to the right of the AMB in the experimental streaming flow in Fig. 5b) weaker than the others.

Thus, we can see that as the number of holes increases, the number of circulations the AMB is trying to generate increases. Each circulation is then more confined as the AMB is attempting to generate more circulations in the same space. Then, rather than generating long thin circulations, smaller rounder circulations are generated which do not stretch as far from the AMB. Thus, the source flow seen dominating beyond the circulations now dominates from closer to the AMB.

Both of these designs produced maximum flow velocities at ultrasound driving frequency of approximately 310 kHz so close to the resonance of 320 kHz for a standard AMB.

In §3, §4 and §5 we have considered AMBs with multiple, but equally sized holes. The additional jest and circulations in their flow fields may make these multi-hole AMBs useful in mixing applications. Next, we will consider an AMB with two differently sized holes, which we propose could be used as a multi-directional swimmer.

6. Two-hole armoured microbubbles with different sized holes

Single-hole AMBs can self-propel when broken off from their tower [3], driven by the strong jet generated by the oscillating bubble. The single-hole AMB is pushed along with the aperture opening at the rear. The strongest jets are observed when the ultrasound driving frequency is close to the resonant frequency of the aperture opening, and the strength decays the further the driving frequency is from the resonance. Extending these observations to an AMB with two holes of different sizes, hypothesises that such an AMB could be used as a multi-directional swimmer. Our idea is that the resonant frequency of both holes would be sufficiently separated, so that one hole only is activated at a first ultrasound driving frequency propelling the AMB

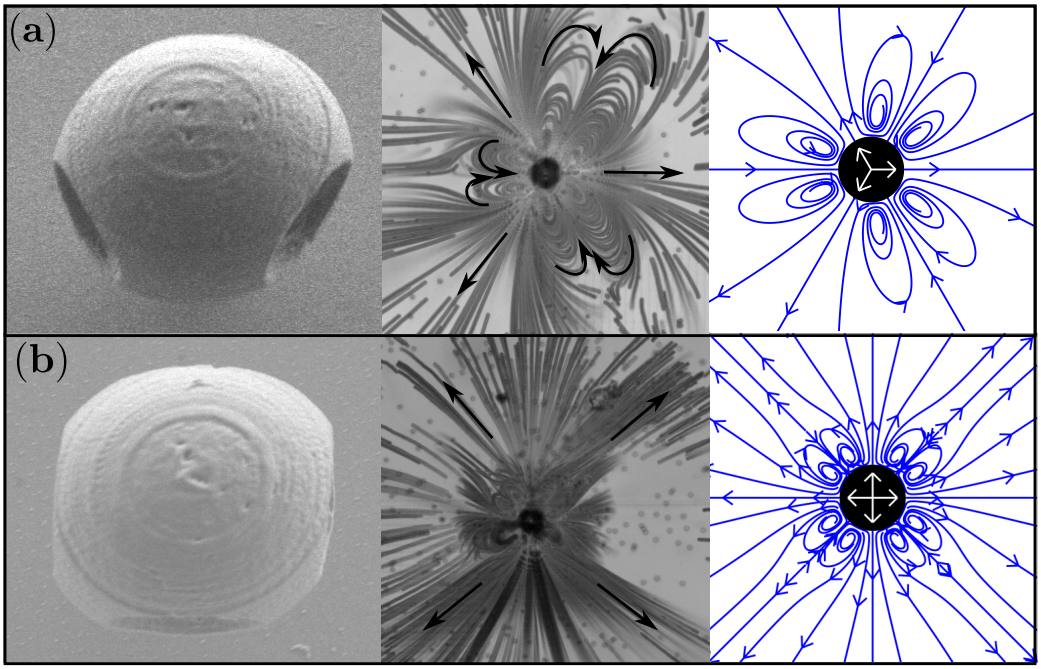

Figure 5: Planar multi-hole AMBs. (a) SEM image of an AMB with three planar holes, the streaming flow generated by this AMB and the theoretical prediction of its streaming flow. (b) SEM image of an AMB with four planar holes, the streaming flow generated by this AMB and the theoretical prediction of its streaming flow.

in one direction away from the first hole, and the other hole only would be activated at a second driving frequency to propel the AMB in a different direction away from the second hole.

For such a swimmer, we would first need to see if two different sized holes on a single AMB can be activated at different frequencies, which is what we will analyse here. We now return to our original two-hole AMB but with the two holes differently sized (Fig. 6). The radii of the holes are 3 μm and 7.5 μm. We have previously reported [3] that the resonant frequency of a single-hole AMB with a 3 μm and 7.5 μm hole are respectively 510 kHz and 160 kHz, which provides an initial estimate for the two resonances of our two-hole AMB.

As anticipated, the large hole dominates at lower frequencies (see Fig. 6e). The streaming flow matches that of a single-hole AMB with two pairs of circulations, one pair in front and one pair behind, with a stronger jet near the large opening (see Fig. 6c). The maximum velocity observed in front of the large hole, in this regime, is observed at 190 kHz, where its relative strength is also visible in videos by the number of tracer particles pulled through this jet (and the distance they start away from the jet) compared to the small hole. The largest flow velocities, in this regime, are only observed over a small range of frequencies.

At larger frequencies, the small hole dominates with the largest velocities observed in front of the small hole at around 330 kHz and slightly later at 360 kHz, a far lower frequency than the 510 kHz for the single-hole AMB with this sized hole. The maximum velocities observed in front of the small hole at 330 kHz are significantly higher than those produced in front of the large hole at 190 kHz (when the large hole dominated). Thus, at intermediary frequencies, there is only a gently drop off in velocity magnitude after the large hole reaches its maximum velocity. Additionally, it is why there is a greater difference in strength between the two holes when the small hole dominates than when the big hole dominates. Increasing the ultrasound driving voltage at lower frequencies and varying this with frequency is one possibility of how to equalise the maximum velocity produced by the small hole when it dominates and the big hole when it dominates.

When the small hole dominates, the streaming flow contains a strong jet in front of the small opening. Near the large hole, we observe a pair of small circulations, with circulations as small as the radius of the AMB having been observed. However, in Fig. 6d no circulations are visible near the small hole, although we do occasionally observe two circulations in this region,

suggesting any circulations are not very stable. This contrasts with an AMB with a single $3\mu m$ radius hole, where experimentally we observe two large elongated circulations near the small hole, in agreement with our numerical prediction for this single-hole AMB. This difference may be attributed to the large hole, as its size means a marked difference between an AMB with a single 3 micrometer hole and the two-hole AMB, as already noted by the substitutional drop in resonance frequency of the small hole.

In the velocity analysis of Fig. 6e, at high frequencies, unexpectedly large velocities are observed near the large hole that do not decay quickly with increasing frequency. However, these high velocities do not correspond to a strong jet, but to the two small (size on the order of the AMB), fast moving circulations near the large hole of the AMB. Additionally, a high density of tracer particles collects in these circulations, reducing the accuracy of our particle tracking analysis here and causing the large oscillation in estimated velocity.

7. Conclusion

In this paper, we have considered AMBs with multiple surface holes, extending previous work on single hole AMBs. With two or three equally spaced in-plane holes, two and three dominating pairs of circulations are observed, but at four holes the circulations become too constrained and in plane radial motion dominates with small circulations only maintained very close to the AMB. 3D spacing of the holes display similar behaviour. This suggests multi-hole AMBs are a useful alternative to multi-propulsor compounds for generating multiple jets and circulations pointing in different directions, with the advantage that multi-hole AMBs are smaller and faster to fabricate. But, hole density limits the number of jets and circulations which can be produced by multi-hole AMBs of a fixed radius so our two and three-hole AMBs show the most promise. These two and three-hole AMBs may be useful in microfluidic mixing due to the additional jets and circulations they generate compared to a single-hole AMB.

Using a two-hole AMB, with holes of size 7.5 μm and 3 μm, we showed the large hole dominated at a low driving frequency around 190 kHz and the small hole at higher driving frequencies around 360 kHz. Although, the small hole produces a stronger streaming flow overall than the large hole, in both cases the dominating hole had a strong jet in front of itself. With a single hole AMB, it was previously demonstrated this jet could self-propel

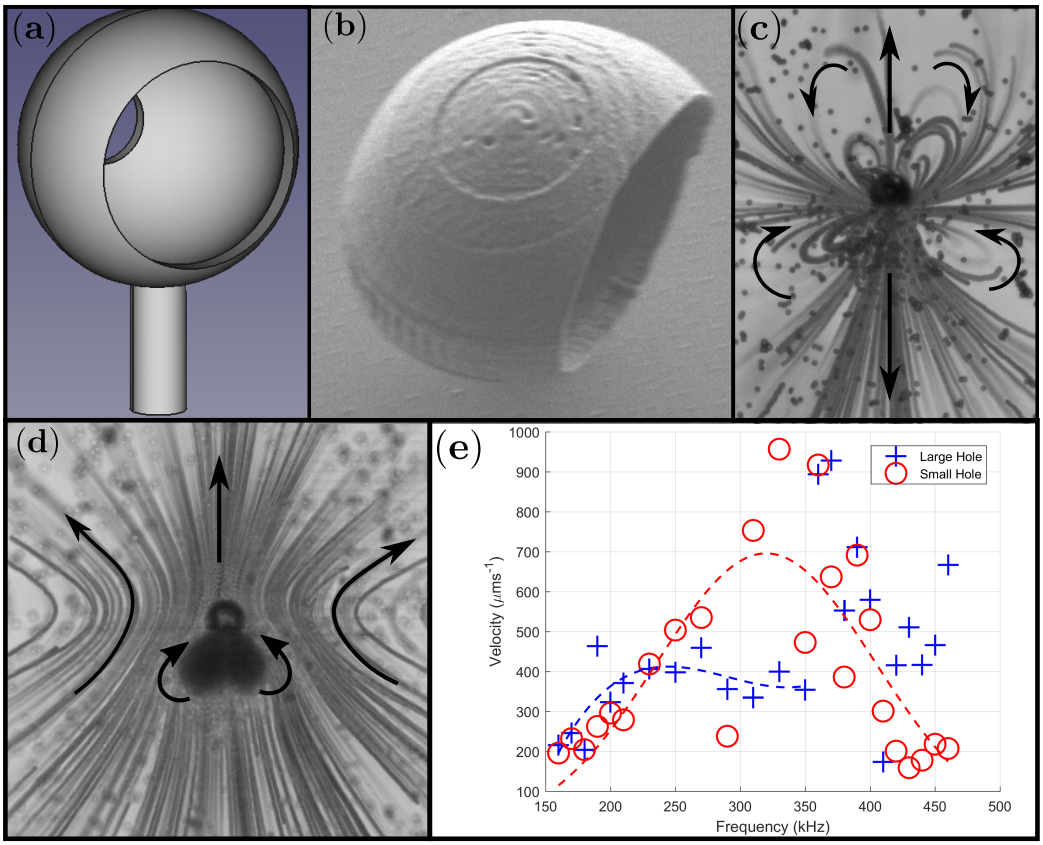

Figure 6: AMB with two different sized holes. (a) FreeCAD design of the AMB. (b) SEM image of this AMB. (c) Experimental streaming flow around this AMB in the regime where the large hole dominates at 180 kHz. (d) Experimental streaming flow around this AMB in the regime where the small hole dominates at 370 kHz. (e) Velocity in front of the large and small hole of the AMB as the driving frequency increases. The velocities are averaged over three AMBs. Crosses and circles mark the experimental data with the dotted lines showing a Bell Curve line of best fit for the small hole and a degree three polynomial of best fit for the large hole below 350 kHz.

an AMB after it has been broken off from its tower [4], so we propose that this two-hole AMB could be used as a multi-directional swimmer (after it has been broken off from its tower). The two-hole swimmer would be operated by changing the ultrasound driving frequency to change its direction. When an ultrasound field of frequency 190 kHz is applied we expect the AMB would swim in the first direction, away from the direction the large hole is pointing in. Then, when an ultrasound field of frequency 360 kHz is applied we expect it would swim the opposite way, away from the direction the small hole is pointing. Future work would be needed to investigate this, which could also investigate adding more, differently sized holes to the AMB to see if this would allow the AMB to swim in more than two directions.

Acknowledgements

T.A.S. would like to thank Prof Eric Lauga for support to travel to the laboratories at the Universite Grenoble Alpes to perform these experiments, including for partial financial support from the European Union's Horizon 2020 research and innovation programme (grant no 682754 to Eric Lauga). T.A.S. also acknowledges a travel grant form the Cambridge Philosophical Society. We thank Thomas Combriat for assistance in using his FAST particle tracking software and Dr Jean-François Louf for providing Python scripts to assist the frequency analysis. We also thank Microlight [10] for support with 3D microfabrication.

Declarations of interest: none

References

[1] Ahmed, D., Lu, M., Nourhani, A., Lammert, P., Stratton, Z., Muddana, H., V.H.Crespi, T.J.Huang, 2015. Selectively manipulable acoustic-powered microswimmers. Sci. Rep. 5, 9744.

[2] Ahmed, D., Mao, X., Juluri, B.K., Huang, T.J., 2009. A fast microfluidic mixer based on acoustically driven sidewall-trapped microbubbles. Microfluid. Nanofluid. 7, 727–731.

[3] Bertin, N., Spelman, T.A., Combriat, T., Hue, H., Stephan, O., Lauga, E., Marmottant, P., 2017. Bubble-based acoustic micropropulsors: active surfaces and mixers. Lab Chip 17, 1515–1528.

[4] Bertin, N., Spelman, T.A., Stephan, O., Gredy, L., Bouriau, M., Lauga, E., Marmottant, P., 2015. Propulsion of bubble-based acoustic microswimmers. Phys. Rev. Applied 4, 064012.

[5] Chen, Y., Lee, S., 2014. Manipulation of Biological Objects Using Acoustic Bubbles: A Review. Integr. Comp. Biol. , 1–10.

[6] Chung, S.K., Cho, S.K., 2008. On-chip manipulation of objects using mobile oscillating bubbles. J. Micromech. Microeng. 18, 125024.

[7] Combriat, T., . http://www-liphy.ujf-grenoble.fr/thomas-combriat-en.

[8] Davidson, B.J., Riley, N., 1971. Cavitation Microstreaming. J. Sound Vib. 15, 217–233.

[9] Feng, J., Yuan, J., Cho, S.K., 2015. Micropropulsion by an acoustic bubble for navigating microfluidic spaces. Lab. Chip 15, 1554–1562.

[10] http://www.microlight.fr, .

[11] Longuet-Higgins, M.S., 1998. Viscous streaming from an oscillating spherical bubble. Proc. Roy. Soc. Lond. A 454, 725–742.

[12] Maksimov, A.O., 2007. Viscous streaming from surface waves on the wall of acoustically-driven gas bubbles. Eur. J. Mech. B-Fluid 26, 28–42.

[13] Marmottant, P., Hilgenfeldt, S., 2003. Controlled vesicle deformation and lysis by single oscillating bubbles. Nature 423.

[14] Marmottant, P., Hilgenfeldt, S., 2004. A bubble-driven microfluidic transport element for bioengineering. Proc. Natl. Acad. Sci. USA 101, 9523–9527.

[15] Marmottant, P., Raven, J.P., Gardeniers, H., Bomer, J.G., Hilgenfeldt, S., 2006. Microfluidics with ultrasound-driven bubbles. J. Fluid Mech. 568, 109–118.

[16] Micro Resist Technology, . Ormocomp®. URL: `https://www.microresist.de/en/products/hybrid-polymers/uv-imprint-uv-moulding/ormocomp%C2%AE`.

[17] Mobadersany, N., Sarkar, K., 2019. Acoustic microstreaming near a plane wall due to a pulsating free or coated bubble: velocity, vorticity and closed streamlines. J. Fluid Mech. 875, 781–806.

[18] Raqeeb, T., Rallabandi, B., Hilgenfeldt, S., 2016. Particle migration and sorting in microbubble streaming flows. Biomicrofluidics 10, 014124.

[19] Spelman, T.A., 2017. Artificial Microdevices: Armoured Microbubbles and a Magnetically Driven Cilium. Ph.D. thesis. University of Cambridge.

[20] Spelman, T.A., Lauga, E., 2016. Arbitrary axisymmetric steady streaming: Flow, force and propulsion. J. Eng. Math , 1–35.

[21] Wang, C., Rallabandi, B., Hilgenfeldt, S., 2013. Frequency dependence and frequency control of microbubble streaming flows. Phys. Fluids 25, 022002.

[22] Xu, Y., Hashmi, A., Yu, G., Lu, X., Kwon, H.J., Chen, X., Xu, J., 2013. Microbubble array for on-chip worm processing. Appl. Phys. Lett. 102, 023702.

Appendix A. Theoretical resonances of bubble bands on a sphere surface

In this appendix, we study how two bands of bubble surface on a sphere effect its resonances, to consider how the separation of two holes effects their interaction.

Our analytic potential model is axisymmetric so limited to at most two holes, which must be positioned at the poles. To overcome the positioning limitation we instead impose two axisymmtetric bands of bubble surface of sector angle $\beta = 0.52$ (although such as set-up is not possible experimentally) to theoretically analyse how the gap between two bubble regions on a spherical surface effects the resonance, see Fig A.1. For a single band (our control), moving its position on the sphere changes Ω (and thus its resonance frequency) but minimally until it is close to the pole. This small change in Ω is expected since the shape of the band will change depending on if the band is close to the pole or the equator. The sharp change near $\alpha = \pi/2 - 0.52$

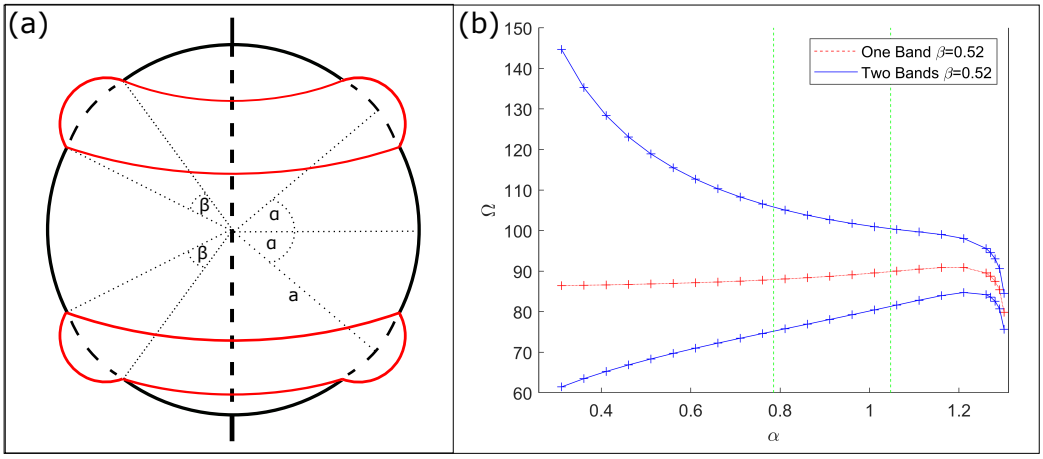

Figure A.1: Analytical study of an AMB with two bands of oscillating bubble surface. (a) Schematic (b) Change in eigenvalue Ω (proportional to f^2) as the bubble bands are separated. The two vertical green lines are at $\alpha = 1.04$ and $\alpha = 0.78$ corresponding to the angle between holes if three or four equally spaces holes respectively are placed around the equator.

occurs as the band approaches the pole, where its internal gap is shrinking to zero so it is tending towards a sharp topological change. However, this indicates that any major changes in resonant frequency as a pair of bands are moved around the sphere (when not very close to the poles) can be attributed to their interactions. Similar to two holes, for two bands, there are two close in-phase and out-of-phase mode one oscillations with a resonance either side of the single-hole resonance. The largest separation and changes to those resonances is at small α when the two bands are close together, thus indicating a strong interaction. However this reduces the further they are away and even at $\alpha = 1.04$ and $\alpha = 0.78$ – corresponding to the spacing for three and four equally spaces holes around the equator – the resonances are still in the region where gaps have limited effect on the resonances which thus implies the effect between them are limited. Similar patterns are seen at other values of β.